Research Square

Preprints are preliminary reports that have not undergone peer review.
They should not be considered conclusive, used to inform clinical practice,
or referenced by the media as validated information.

A Simplified Method for Seismic Fragility Analysis of Geogrid-Encased Stone Column Composite Foundations

Xiaocong Cai
Hunan University
Ling Zhang
zhanglhd@hnu.edu.cn
Hunan University
Jinpeng Tan
Hunan University
Zijian Yang
Hunan University

Research Article

Keywords: Geogrid-Encased Stone Column, Ultimate Seismic Bearing Capacity, Seismic Fragility, Limit Equilibrium Method, Machine Learning, Shaking Table Test

Posted Date: August 26th, 2026

DOI: https://doi.org/10.21203/rs.3.rs-10673954/v1

License: This work is licensed under a Creative Commons Attribution 4.0 International License.
Read Full License

Additional Declarations: No competing interests reported.

A Simplified Method for Seismic Fragility Analysis of Geogrid-Encased Stone Column Composite Foundations

Abstract

Geogrid-encased stone columns (GESCs) are increasingly utilized in earthquake-prone areas, yet a practical framework for quantifying their seismic fragility remains underdeveloped. This study develops a machine learning-based probabilistic assessment framework for the seismic fragility analysis of GESC composite foundations. The framework employs a validated analytical model for estimating the ultimate seismic bearing capacity, which is then integrated with the Monte Carlo simulation to account for the inherent uncertainties. A comprehensive parametric study is conducted to systematically evaluate the influence of seismic coefficients (k_h and k_v), column diameter (D_c), tensile strength (T), area replacement ratio (m), shear strength (φ_c, c_c, φ_s, c_s), vertical load demand (P_v), footing width (B), overburden pressure (q_1), and shear strength utilization ratio (n). Results demonstrate that the parameters φ_s and k_v/k_h are the most influential on the failure probability (P_f), whereas D_c and c_c have a negligible effect. P_f shows a positive correlation with T, m, φ_c, c_c, φ_s, c_s, B, and q_1, and a negative correlation with k_v/k_h, D_c, and P_v. Since the seismic reliability is more critically influenced by native soil conditions than by column enhancements, the design shall focus on key parameters: high-strength geogrids, adequate foundation width, a high are replacement ratio, and a dense arrangement of small-diameter columns.

Keywords: Geogrid-Encased Stone Column; Ultimate Seismic Bearing Capacity; Seismic Fragility; Limit Equilibrium Method; Machine Learning; Shaking Table Test.

1. Introduction

Soft soil deposits pose significant geotechnical challenges for construction, particularly in seismically active regions, due to their low bearing capacity, high compressibility, and potential for liquefaction. Ordinary stone column (OSC) improvement is a widely adopted ground reinforcement technique that enhances soil stiffness, increases bearing capacity, and accelerates consolidation (Chen et al., 2022; Gu et al., 2022a; Gu et al., 2022b; Pandey et al., 2022). However, in extremely soft soils, the lack of adequate lateral confinement often leads to excessive bulging and premature failure of OSCs. The geogrid-encased stone column (GESC) effectively mitigates this issue through the substantial additional confinement provided by the geogrid to the column (Abid et al., 2023; Liu et al., 2023; Mohamed et al., 2023; Zeini et al., 2023). The geogrid-encased stone columns (GESCs) allow for the full-strength mobilization of the column material and a marked improvement in the overall load-deformation response of the foundation system (Bahi and Houhou, 2024; Castro Gonzalez et al., 2024; Elwakeel and Elsherbini, 2024; Hosseinpour, 2024).

While the static performance of GESC foundations has been extensively studied through analytical (Kong et al., 2018; Pulko and Logar, 2017; Zhang et al., 2012), numerical (Ji et al., 2024; Qin et al., 2024; Yousuf and Samadhiya, 2024; Zhang et al., 2024), and experimental (Kang et al., 2024; Modalavalasa and Ramanathan, 2024; Pandey Balbir et al., 2024; Yoosefi et al., 2024) methods, their response under seismic loading remains a complex and less quantified aspect. Earthquakes impose cyclic and dynamic stresses that threaten stability through mechanisms such as reduced lateral confinement, the generation of excess pore water pressure in surrounding soil, and complex inertial interactions. Consequently, the seismic bearing capacity emerges as a critical, yet insufficiently defined, design parameter. Current methodologies for OSC composite foundations predominantly employ limit equilibrium methods to assess ultimate seismic bearing capacity (Nav et al., 2020; Nayak et al., 2020; Pandey et al., 2020; Tan et al., 2020; Thakur et al., 2020a, b). The geogrid encasement decreases the column's dependence on the surrounding soil while simultaneously introducing greater complexity into the failure mechanisms and computational methods. Nevertheless, existing research on GESCs under dynamic conditions has primarily relied on laboratory tests (Cengiz and Guler, 2018a, b, 2020; Ji et al., 2025; Lakkimsetti and Latha, 2024; Ou Yang et al., 2021) and numerical simulations (Cai et al., 2025; Dinesh et al., 2024; Zhang et al., 2025). These studies have focused on characterizing the dynamic

response in terms of deformation, acceleration, stress distribution, and pore water pressure evolution. However, such deterministic approaches cannot inherently account for the significant uncertainties prevalent in geotechnical systems—including the spatial variability of soil properties, the inherent randomness in material strengths, and the uncertainty in seismic demand. Therefore, a purely deterministic safety factor may not adequately represent the real risk of failure under seismic events of varying intensities.

To address these uncertainties, fragility analysis has emerged as a powerful probabilistic framework for seismic risk assessment, forming the backbone of performance-based earthquake engineering. It quantifies the conditional probability of exceeding a specific limit state (e.g., bearing capacity failure) given a seismic intensity measure. Nevertheless, the application of this probabilistic framework to GESC composite foundations is scarcely reported in the literature (Cai et al., 2026; Qiu et al., 2025). Current seismic performance evaluations, when attempted, often rely on complex, computationally expensive finite-element models coupled with dynamic analysis (Geng et al., 2017; Tang et al., 2015). Such sophisticated analyses, while valuable, may hinder practicality for routine design, parametric studies, and reliability-based optimization. This highlights a clear need for a analytical methodology that can efficiently generate seismic fragility curves for GESC foundations while explicitly incorporating parameter uncertainty.

This study develops a machine learning-based probabilistic assessment framework for the seismic fragility analysis of GESC composite foundations. The calculation method of ultimate seismic bearing capacity is established based on the limit equilibrium method and the equivalent are method, and validated through previous analytical solutions, shaking table test, and field tests. The proposed neural network model integrates the validated analytical model and Monte Carlo simulation, considering parameter uncertainty, for investigating the seismic fragility of GESC composite foundations. A comprehensive parametric study is conducted to investigate the influence of critical factors, including seismic coefficients (k_h and k_v), column diameter (D_c), tensile strength (T), area replacement ratio (m), shear strength (φ_c, c_c, φ_s, c_s), vertical load demand (P_v), footing width (B), overburden pressure (q_1), and shear strength utilization ratio (n).

2. Calculation of Seismic Bearing Capacity

2.1. Seismic Bearing Capacity Model

Fig. 1 presents a footing resting on a foundation under static loading. The ultimate static bearing capacity (P_L) of a foundation under a circular footing can be calculated based on the classical Terzaghi bearing capacity theory, as follows:

$$P_L = 1.2c_sN_c + q_1N_q + 0.3\gamma_sBN_\gamma \tag{1}$$

where, N_c, N_q, and N_γ are static bearing capacity factors; q_1 is the overburden pressure; B is the width (or diameter) of the footing; $q_1 = \gamma_s h_0$ is the overburden pressure; h_0 is the embedded depth of the footing; c_s, φ_s, and γ_s are the cohesion, angle of internal friction, and weight of the foundation soil, respectively.

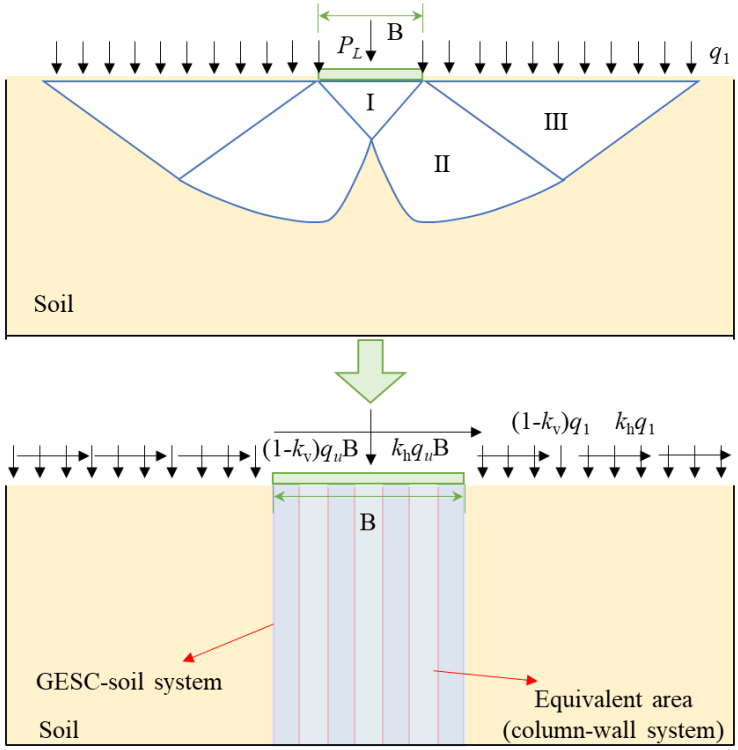


Fig. 1. Schematic diagram of the GESCs composite foundation under static and seismic loading.

To evaluate the ultimate seismic bearing capacity of the GESC composite foundation, an equivalent area (Hassen et al., 2013; Zheng et al., 2020) method is commonly used. The composite properties of the GESC composite foundation are defined by weighted averaging as follows:

$$c = (1-m)c_s + m(c_c + c_g) \tag{2}$$

$$tan\varphi = (1-m)tan\varphi_s + mtan\varphi_c \tag{3}$$

$$\gamma = (1-m)\gamma_s + m\gamma_c \tag{4}$$

where, m is the area replacement ratio; c_g is apparent cohesion provided by geogrid encasement; c, φ, and γ are the cohesion, angle of internal friction, and weight of the composite foundation, respectively; c_c, φ_c, and γ_c are the cohesion, angle of internal friction, and weight of the column material, respectively. The same method for the bearing capacity calculation of ordinary stone column (OSC) composite foundations was applied as described in the previous study (Zheng et al., 2020). Further extending this method to the calculation of the ultimate seismic bearing capacity of GESC composite foundation, the apparent cohesion (c_g = Ttan(45°+φ_c/2)/D_c) due to additional confinement provided by geogrid encasement is incorporated into the proposed model (T and D_c are the geogrid tensile strength and the column diameter, respectively). The horizontal (k_h = α_h/g) and vertical (k_v = α_v/g) acceleration coefficients are normalized by gravitational acceleration (g) to quantify the earthquake-induced inertial forces (α_h and α_v are the horizontal and vertical peak ground acceleration, respectively). Consequently, the ultimate seismic bearing capacity (q_u) of the GESC composite foundation is rewritten as:

$$q_u = 1.2cN_{cE} + q_1N_{qE} + 0.3\gamma BN_{\gamma E} \tag{5}$$

where, N_{cE}, N_{qE}, and $N_{\gamma E}$ are seismic bearing capacity factors.

2.2. Determination of Seismic Bearing Capacity Factors

Under seismic loading, the failure surface tends to move upwards. Fig. 2 (a) presents the actual and simplified failure mode of the GESC composite foundation subjected to seismic loading. The simplified failure region can be divided into abc and bcd blocks. The geometry relationship can be expressed as:

$$\begin{cases} |ab| = B \\ |bc| = Btan\alpha_{comp} \\ |dc| = Btan\alpha_{comp}/sin\alpha_s \\ |bd| = Btan\alpha_{comp}/tan\alpha_s \end{cases} \tag{6}$$

where, α_{comp} and α_s are the critical angles of the active and passive zone, respectively. The calculational formulas recommended by Budhu and Al-Karni (1993) can be rewritten as:

$$\alpha_{comp} = a_{comp} + tan^{-1}\left(\frac{\sqrt{1+tan^2a_{comp})[1+tan(\delta_1+\theta)cota_{comp}]}-tana_{comp}}{1+tan(\delta_1+\theta)(tana_{comp}+cota_{comp})}\right) \tag{7}$$

$$\alpha_s = -a_s + tan^{-1}\left(\frac{\sqrt{1+tan^2 a_s)[1+tan(\delta_2-\theta)cota_s]}+tana_s}{1+tan(\delta_2+\theta)(tana_s+cota_s)}\right) \quad (8)$$

where, $a_{comp} = \varphi - \theta$; $a_s = \varphi_s - \theta$; $\theta = tan^{-1}(k_h/(1-k_v))$ is the seismic angle; δ_1 and δ_2 are the half of the internal friction angle in different regions, respectively.

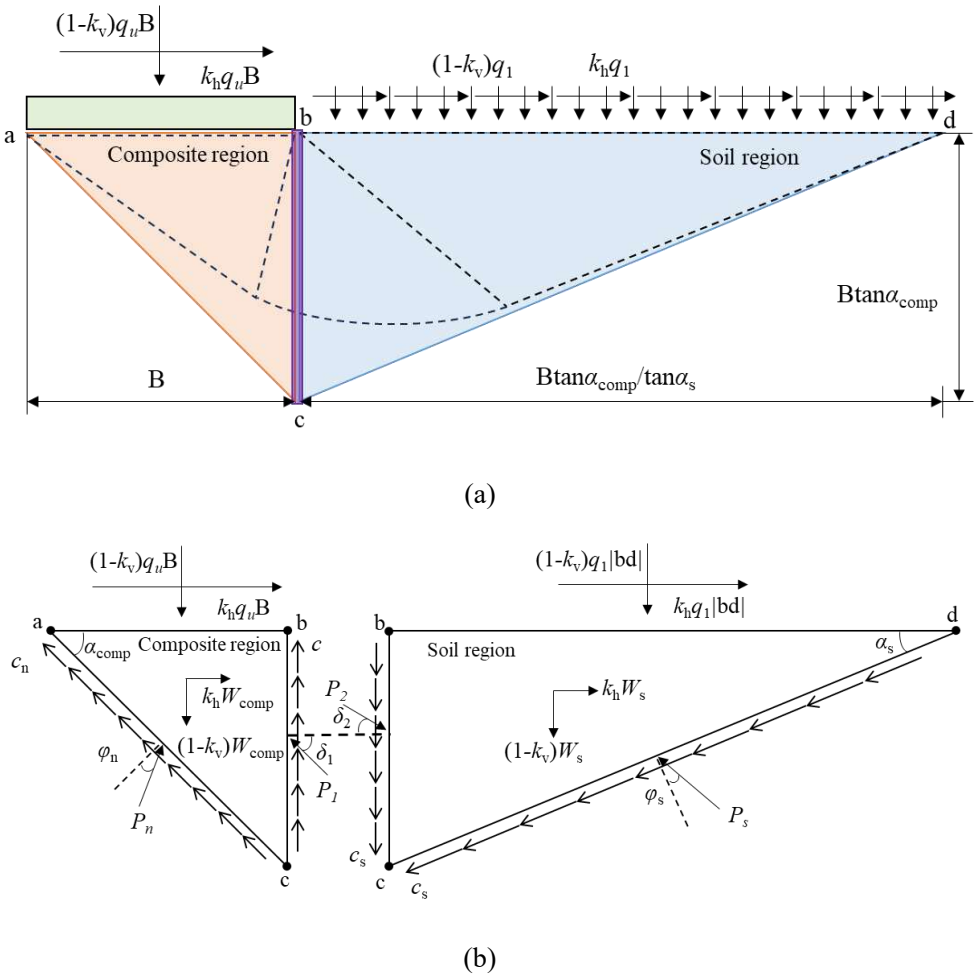


Fig. 2. Calculation mode of GESC composite foundation under seismic loading: (a) failure mode and (b) force analysis.

Fig. 2 (b) presents the force analysis of the different sliding blocks. Assuming $c \neq 0$ and $\gamma = q_1 = 0$, all forces took the moment for the c point:

$$k_h q_u B|bc| - \frac{1}{2}(1-k_v)q_u\, B|ab| - \frac{1}{2}P_s\, cos\varphi_s|dc| + \frac{1}{2}P_n\, cos\varphi_n|ac| = 0 \quad (9)$$

where, $\varphi_n = n\varphi$ and $c_n = nc$ are the angle of internal friction and cohesion of an ac edge, respectively; n is the shear strength utilization ratio. The following equations can be derived from the balance of vertical and horizontal forces:

$$k_h q_u B - c_n cos\alpha_{comp}|ac| - c_s cos\alpha_s|dc| - P_s\, sin(\alpha_s + \varphi_s) + P_n\, sin\left(\alpha_{comp} - \varphi_n\right) = 0 \quad (10)$$

$$k_h q_u B - c_n sin\alpha_{comp}|ac| + c_s in\alpha_s|dc| - P_s\, cos(\alpha_s + \varphi_s) - P_n\, cos\left(\alpha_{comp} - \varphi_n\right) = 0 \quad (11)$$

Organizing the above equation, q_u and N_{cE} can be obtained:

$$q_u = \frac{c_n|bc|cos\varphi_n\left(cos\left(\alpha_{comp}+\alpha_s+\varphi_s\right)|bc|+cos\varphi_s|dc|\right)+c_s|dc|cos\varphi_s\left(cos\varphi_n|ac|+cos\left(\alpha_{comp}+\alpha_s-\varphi_n\right)|dc|\right)}{B(1-k_v)\left(Bsin\left(\alpha_{comp}+\alpha_s+\varphi_s-\varphi_n\right)-sin(\alpha_s+\varphi_s)cos\varphi_n|ac|+sin\left(\alpha_{comp}-\varphi_n\right)cos\varphi_s|dc|\right)-} \quad (12)$$
$$Bk_h\left(2|bc|sin\left(\alpha_{comp}+\alpha_s+\varphi_s-\varphi_n\right)-cos(\alpha_s+\varphi_s)cos\varphi_n|ac|-cos\left(\alpha_{comp}-\varphi_n\right)cos\varphi_s|dc|\right)$$

$$N_{cE} = \frac{c_n|bc|cos\varphi_n\left(cos\left(\alpha_{comp}+\alpha_s+\varphi_s\right)|bc|+cos\varphi_s|dc|\right)+c_s|dc|cos\varphi_s\left(cos\varphi_n|ac|+cos\left(\alpha_{comp}+\alpha_s-\varphi_n\right)|dc|\right)}{cB(1-k_v)\left(Bsin\left(\alpha_{comp}+\alpha_s+\varphi_s-\varphi_n\right)-sin(\alpha_s+\varphi_s)cos\varphi_n|ac|+sin\left(\alpha_{comp}-\varphi_n\right)cos\varphi_s|dc|\right)-} \quad (13)$$
$$cBk_h\left(2|bc|sin\left(\alpha_{comp}+\alpha_s+\varphi_s-\varphi_n\right)-cos(\alpha_s+\varphi_s)cos\varphi_n|ac|-cos\left(\alpha_{comp}-\varphi_n\right)cos\varphi_s|dc|\right)$$

Based on the Mononobe-Okabe formula, the value of the active (K_{AE}) and passive (K_{PE}) earth pressure coefficient from Budhu and Al-Karni (1993) can be rewritten:

$$K_{AE} = \frac{\cos^2(\varphi_{average} - \theta)}{\cos\theta\cos(\delta_1+\theta)\left\{1+\sqrt{\frac{\sin(\varphi_{average}+\delta_1)\sin(\varphi_{average}-\theta)}{\cos(\delta_1+\theta)}}\right\}^2} \quad (14)$$

$$K_{PE} = \frac{\cos^2(\varphi_{average} - \theta)}{\cos\theta\cos(\delta_2+\theta)\left\{1-\sqrt{\frac{\sin(\varphi_{average}+\delta_2)\sin(\varphi_{average}-\theta)}{\cos(\delta_2+\theta)}}\right\}^2} \quad (15)$$

where, $\varphi_{average}$ is the average value of the internal friction angle of the system.

Assuming $q_1 \neq 0$ and $\gamma = c = 0$, the following equations derived from the horizontal force balance of the bc edge can be obtained:

$$K_{AE} q_u |bc| = K_{PE} q_1 |bc| \quad (16)$$

$$q_u = q_1 K_{PE}/K_{AE} \quad (17)$$

$$N_{qE} = K_{PE}/K_{AE} \quad (18)$$

Assuming $\gamma \neq 0$ and $q_1 = c = 0$, the following equations derived from the horizontal force balance of the bc edge can be obtained:

$$q_u K_{AE}|bc| + \gamma|bc|^2 K_{AE}/2 = \gamma_s|bc|^2 K_{PE}/2 \quad (19)$$

$$q_u = |bc|\left(\frac{\gamma_s K_{PE} - \gamma K_{AE}}{2K_{AE}}\right) \quad (20)$$

$$N_{\gamma E} = |bc|\left(\frac{\gamma_s K_{PE} - \gamma K_{AE}}{0.6\gamma B K_{AE}}\right) \quad (21)$$

2.3. Validation of Seismic Bearing Capacity Factors

Three seismic bearing capacity factors are calculated and compared with previous studies (Cai et al., 2026; Richards et al., 1993; Soubra, 1997) for homogeneous cohesionless soil. Fig. 3 (a), (b), and (c) show the calculation results of N_{cE}, N_{qE}, and $N_{\gamma E}$, respectively. Good consistency between present and previous results is observed, demonstrating the feasibility and accuracy of this method.

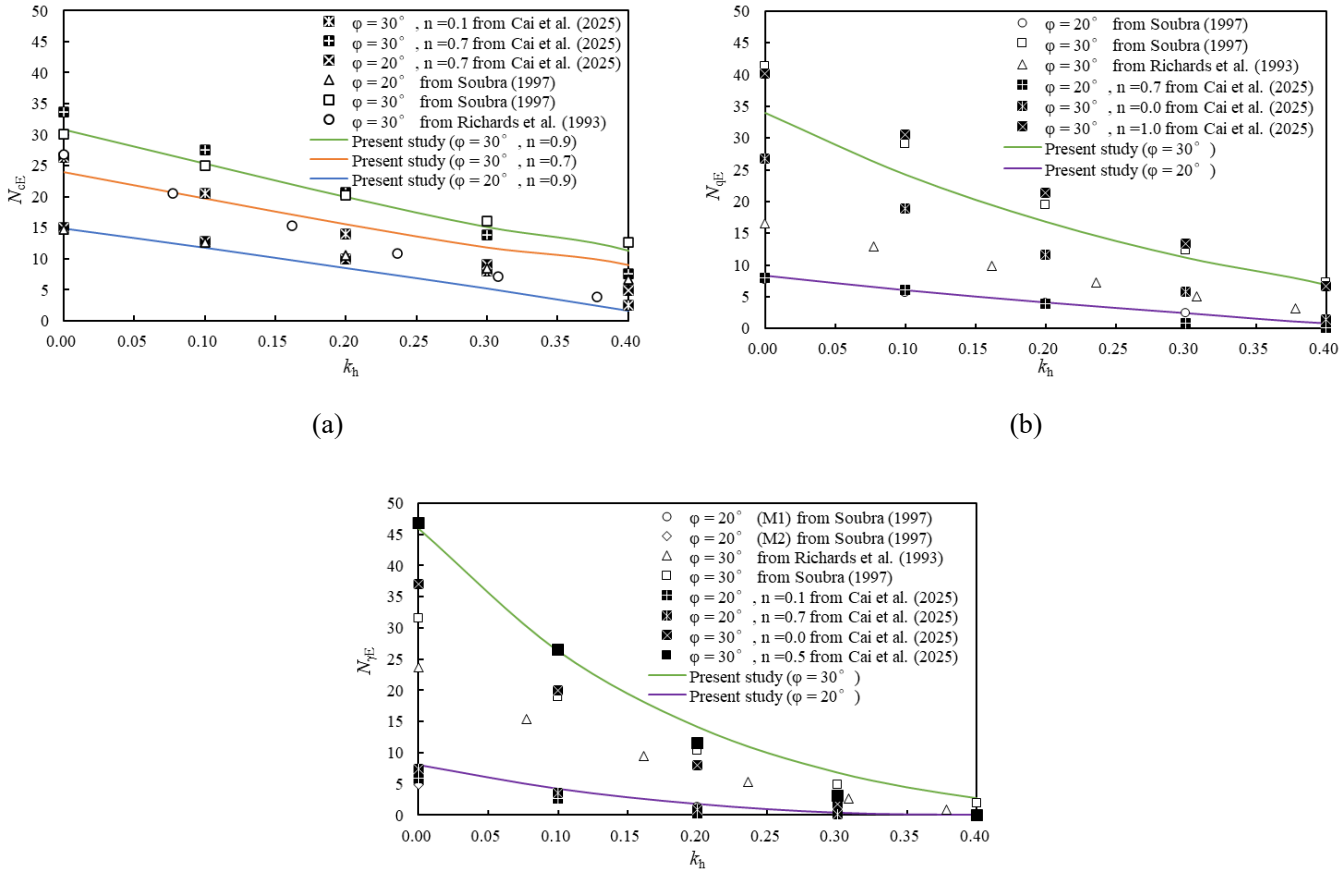


Fig. 3. Comparison of different methods for calculating seismic bearing capacity factors: (a) N_{cE}, (b) N_{qE}, and (c) $N_{\gamma E}$.

2.4. Shaking Table Tests and Field Tests Validation

To further validate the reliability of the proposed method, its predictions for ultimate bearing capacity are compared with experimental data from shaking table and field tests. The 1:10 scale shaking table tests were conducted by Cai et al. (2026) to validate the theoretical model accuracy during seismic loading. The column diameter (D_c) and length (L_c) in shaking table tests are 40 mm and 500 mm, respectively. The geogrid with a tensile strength of about 2~7 kN/m is used to encase the stone aggregates. Table 1 summarizes the parameters

for calculating the seismic bearing capacity of OSC and GESC composite foundations in shaking table tests. Fig. 4 (a) presents the q_u calculation results of OSC and GESC composite foundations under different seismic intensities. The q_u typically increases with increasing tensile strength of geogrid encasement and decreasing k_h. The geogrid encasement significantly increases the q_u of OSC. The close agreement between the present results and previous data further validates the feasibility and accuracy of the proposed method.

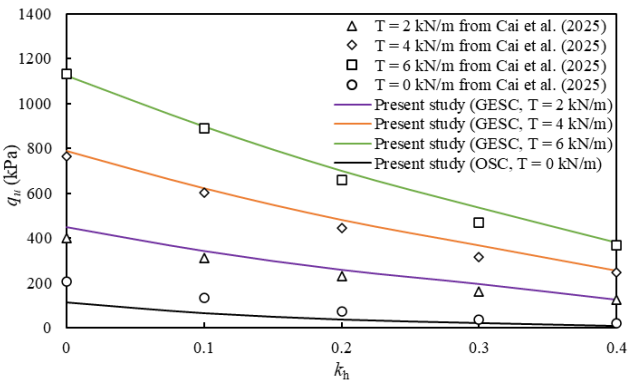
Table 1. Parameter for seismic bearing capacity calculation in shaking table tests.

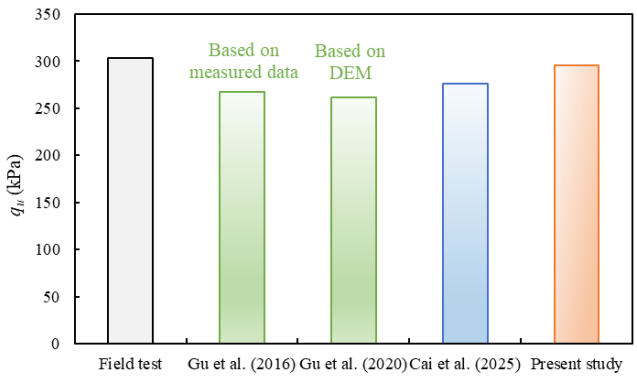
Parameter	Weight	Cohesion	Angle of internal friction	Area replacement ratio	Width of footing	Shear strength utilization ratio
Sand	γ_s = 18 kN/m^3	c_s = 1 kPa	φ_s = 33.68°	m = 16%	B = 0.1 m	n = 0.6
OSC/GESC	γ_c = 17 kN/m^3	c_c = 1 (or 1 + c_g) kPa	φ_c = 41.70°			

In the field tests, the geogrid with a tensile strength of about 30 kN/m and an aperture dimension of 40 mm × 40 mm is used to encase the stone aggregates. The width of the footing is 1.2 m, and the area replacement ratio is about 13.64%. The end-bearing columns with a diameter of 0.5 m and an internal friction angle of 40°are used to reinforce the soft soil with a cohesion of 15 kPa. The radial stress coefficient (K_p) method is commonly used to calculate the static bearing capacity of such columns (Gu et al., 2020; Gu et al., 2016), as follows:

$$q_u = (\sigma_{r0} + 4c_s + \sigma_{rg})\, K_p \tag{22}$$

where, $\sigma_{r0} = 2c_u$ is the initial radial stress; $\sigma_{rg} = 2T/D_c$ is the confining stress provided by the geogrid encasement. The q values from field tests, Gu et al. (2020), Gu et al. (2016), Cai et al. (2026), and the present study are presented in Fig. 4 (b). The bearing capacity difference is successively -11.66%, -13.80%, -8.98%, and -2.48% compared to the field test results. A more precise result is obtained from the present study compared to the other solutions.





(a) (b)

Fig. 4. Seismic bearing capacity calculation of composite foundation based on: (a) shaking table test and (b) field test.

3. Seismic Fragility Analysis

3.1. Definition of Failure Discrimination

The ultimate seismic bearing capacity (q_u) of GESC composite foundation is calculated using the validated model described in Section 2. A performance criterion is then defined: the foundation is considered unsatisfactory if q_u is less than the vertical load demand (P_v); otherwise, its performance is deemed satisfactory. The representative vertical load demand of about 75 kPa is adopted for the superstructure in the present study based on the literature review (Abid et al., 2023; Bahrami and Marandi, 2021; Farah and Nalbantoglu, 2020; Gu et al., 2025; Gu et al., 2022b; Gu et al., 2016; Menon and Bhasi, 2024; Nayak et al., 2019; Ou Yang et al., 2021; Qiu et al., 2025; Rathod et al., 2021; Sadr and Hataf, 2021; Zhou et al., 2019). In geotechnical engineering and composite foundation research, a representative standard load value is often selected to facilitate comparison and discussion across different studies. The P_v value is a widely adopted typical or reference value in numerous publications on stone columns. As the q_u is influenced by multiple uncertain factors (e.g., seismic loading, material properties, and model configuration), it is not a deterministic value. Thus, evaluating seismic safety necessitates a probabilistic approach via fragility functions, which quantify the seismic failure probability of GESC composite foundations.

3.2. Parameter Selection

A parameter treatment strategy is implemented to simplify the seismic fragility analysis. Parameters exhibiting negligible expected variation (e.g., material unit weights) or with a standardized influence are assigned fixed constant values. Therefore, the γ_s, γ_c, q_1, B, $k_{v,}$ and n are 18 kN/m^3, 20 kN/m^3, 10 kPa, 1 m, 0.5k_h, and 0.1, respectively. For the main random variables (e.g., φ_c, c_c, φ_s, c_s, T, m, and D_c) with the normal distribution governing system response, a benchmark analysis is defined using central values. The mean value of φ_c, c_c, φ_s, c_s, T, m, and D_c from their specified ranges are 40°, 25°, 10 kPa, 15 kPa, 0.15, 100 kN/m, and 0.8 m, respectively. k_h is considered to obey the uniform distribution in the present study. Table 2 summarizes the parameters for seismic fragility analysis.

Table 2. Summary of statistical uncertain parameters for seismic fragility analysis.

Parameter	Distribution	Range	Mean	References
φ_c	Normal distribution	35°~45°	40°	Alonso and Jimenez (2011)
φ_s	Normal distribution	10°~30°	25°	Zhang et al. (2017)
c_c	Normal distribution	0~20 kPa	10 kPa	Zhang et al. (2017)
c_s	Normal distribution	5~30 kPa	15 kPa	Zhang et al. (2017)
m	Normal distribution	0.10~0.35	0.15	Yoo and Abbas (2019) and Bazzazian Bonab et al. (2020)
T	Normal distribution	10~400 kN/m	100 kN/m	Yoo and Abbas (2020) and Bhandari and Han (2010)
D_c	Normal distribution	0.4~1.2 m	0.8 m	Mahawish et al. (2021)

3.3. Calculation Methodology

A neural network model is implemented in MATLAB to predict the failure probability of GESC foundations, with explicit consideration of input parameter uncertainties. The selection of input parameters followed a two-step procedure. First, parameters that significantly influence the q_u or exhibit substantial uncertainty are identified based on the findings in Section 2. Second, the reasonable ranges and statistical distributions for these parameters are established through a comprehensive literature review observed in Section 3.2. A dataset in the form of a 7 × N array is generated, corresponding to the seven input parameters listed in Table 2. For each input parameter, N random samples are drawn to calculate the corresponding q_u. These q_u values will be compared with the P_v from Section 3.1. Based on the definition of failure discrimination, the samples are labeled and classified. Finally, a neural network (Fig. 5) with input, hidden, and output layers is constructed (i.e., structure is 9-32-16-8-1) to perform regression and predict the failure probability (P_f) of GESC composite foundations under varying conditions.

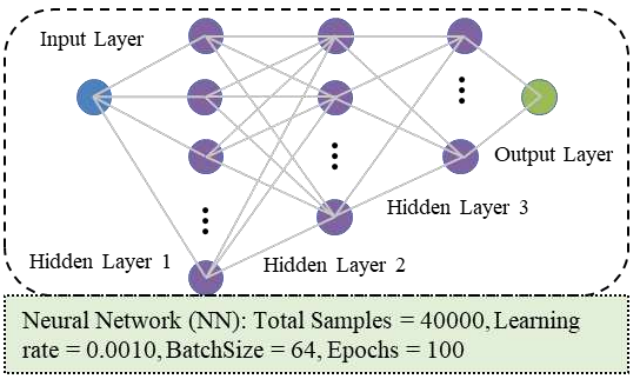
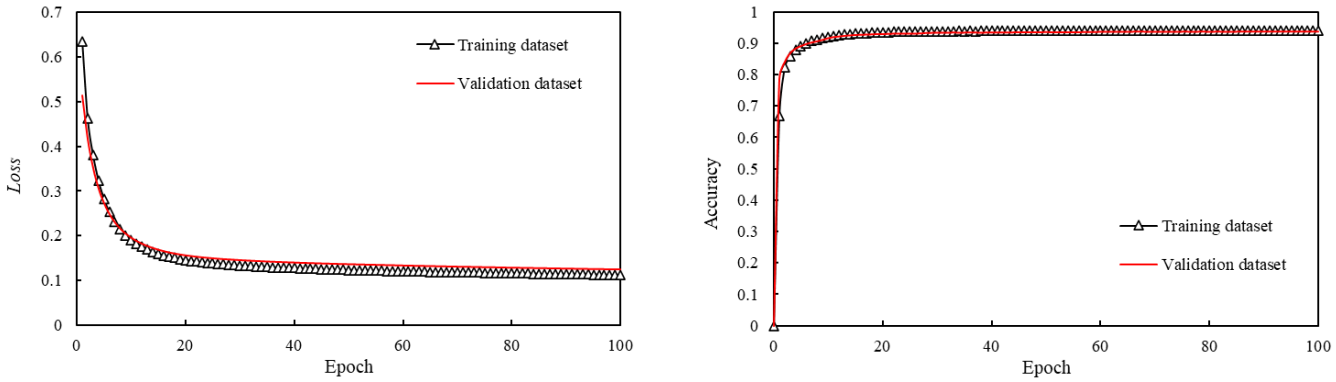


Fig. 5. Neural network model.

3.4. Model Verification

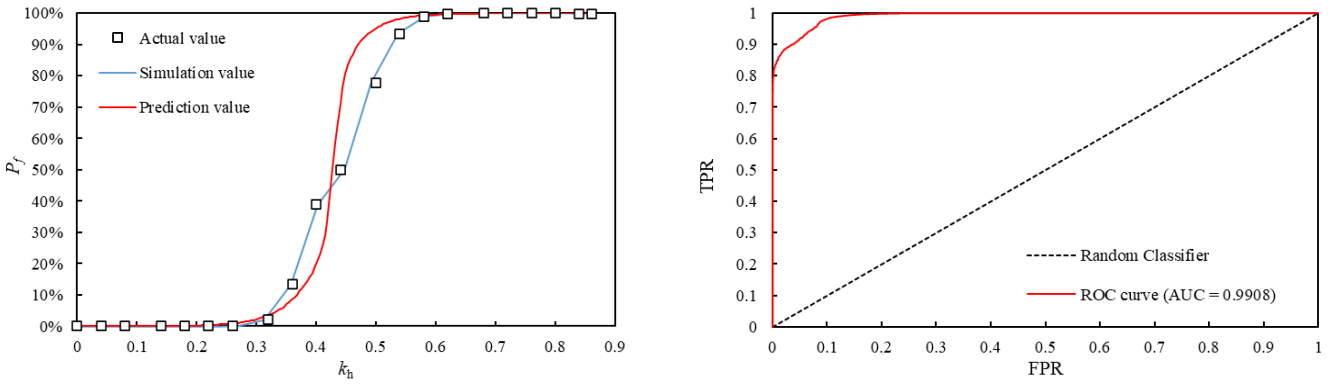
Fig. 6 (a) illustrates the variation of loss values with the number of epochs, with a clear decreasing trend observed. The decreasing loss values with the increasing number of training epochs directly reflect the normal learning and convergence process of machine learning models. The underlying mechanism lies in the model's iterative optimization, which continuously adjusts its internal parameters to achieve increasingly accurate fitting of the training data. The loss value of approximately 0.1241 is obtained with the increasing iteration times from 0 to 100. Fig. 6 (b) depicts the evolution of model accuracy with respect to the number of epochs. The model accuracy exhibits a trend of improvement with increasing training epochs, achieving a value of about 93.83% at 100 epochs. The proposed neural network model with a low loss value and high accuracy guarantees its reliability and rationality.



(a) (b)

Fig. 6. Effect of iteration times on the: (a) loss curves and (b) accuracy curves.

To validate the accuracy of seismic fragility analysis, the failure probability curves from different methods is given in Fig. 7 (a). The prediction curve shows a good consistency compared to the actual values and simulation results. Fig. 7 (b) presents the ROC (Receiver Operating Characteristic) curve used to evaluate the performance of a binary classification model. ROC curve demonstrates the classifier's ability to handle the relationship between true positives and false positives by plotting the model's performance changes across different discriminative thresholds. Horizontal axis represents the false positive rate (FPR) and vertical axis represents the true positive rate (TPR). ROC curve is positioned very close to the upper left corner, indicating that the model achieves an exceptionally high true-positive rate (TPR) while maintaining an extremely low false-positive rate (FPR). The AUC value reaches 0.9908, indicating that the classification model depicted in the figure possesses exceptional discrimination capability and remarkable predictive accuracy.



(a) (b)

Fig. 7. Effect of k_h on failure probability.

4. Parametric Analysis

The effect of different factors (k_v/k_h, D_c, T, m, φ_c, c_c, φ_s, c_s, P_v, B, q_1, and n) on the P_f is investigated in this section. The original parameters in Section 3 are unchanged except for the parameters being studied. Table 3 summarizes the parameters for investigating the variation of P_f.

Table 3. Summary of parameters for P_f calculation.

Parameter	Value	Parameter	Value	Parameter	Value
k_v/k_h	0.2, 0.4, 0.6, and 0.8	φ_c (°)	38, 40, 42, and 45	P_v (kPa)	50, 100, 150, and 200
D_c (m)	0.4, 0.6, 0.8, and 1.0	φ_s (°)	10, 20, 25, and 30	B (m)	2, 5, 8, and 10
T (kN/m)	10, 50, 100, and 200	c_c (kPa)	5, 10, 20, and 50	q_1 (kPa)	50, 100, 200, and 300
m	25%, 30%, 35%, and 40%	c_s (kPa)	5, 10, 15, and 20	n	0.2, 0.4, 0.6, and 0.8

4.1. Effect of k_v/k_h

Fig. 8 presents the effect of k_v/k_h on the P_f. The failure probability increases with increasing k_h and k_v. An increase in k_h generates a stronger horizontal inertial force. This significantly elevates the shear stress between the column and the surrounding soil, resulting in a more significant horizontal displacement, even bending and shear failure. Horizontal forces increase the circumferential tensile and extraction forces of the geogrid, weakening its lateral restraint effect. An increase in k_v generates additional vertical seismic forces, significantly elevating the instantaneous vertical load on the foundation, which may exceed the vertical bearing capacity of the composite foundation. Intense vertical vibration causes a sharp increase in pore water pressure and reduction in effective stress, resulting in soil softening or even liquefaction. This significantly diminishes the lateral support provided by the surrounding soil and substantially reduces the overall stiffness

and bearing capacity of the foundation. In actual earthquakes, combined horizontal and vertical loading leads to the foundation simultaneously facing multiple adverse conditions. These cumulative effects systematically increase the failure probability of the entire composite foundation system.

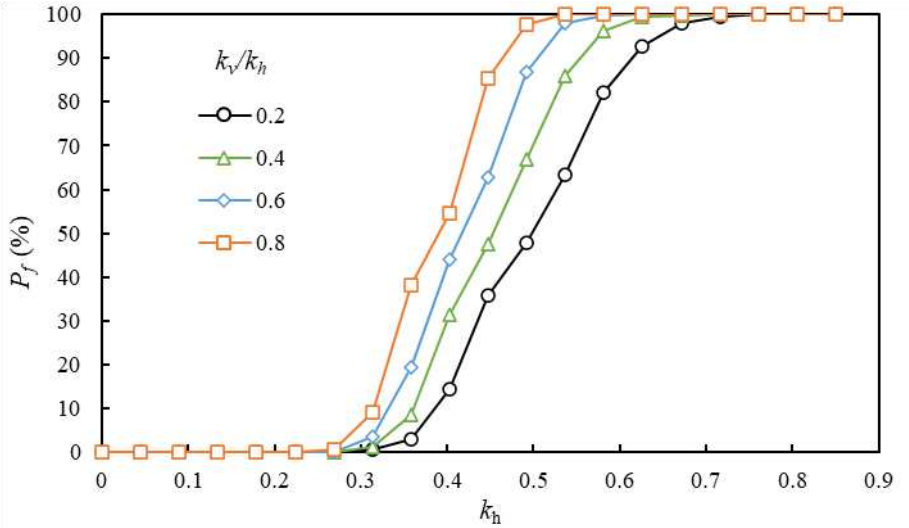


Fig. 8. Effect of k_v/k_h on failure probability.

4.2. Effect of D_c

Fig. 9 presents the effect of D_c on the P_f. The failure probability increases with increasing D_c. An increasing column mass typically under the same seismic acceleration experiences greater horizontal inertial forces, resulting in bending and shear deformation. An increased column diameter typically indicates greater column stiffness, which may concentrate more seismic shear forces. For large-diameter columns, the confinement demand increases at a much higher rate than the capacity improvement, elevating the failure probability.

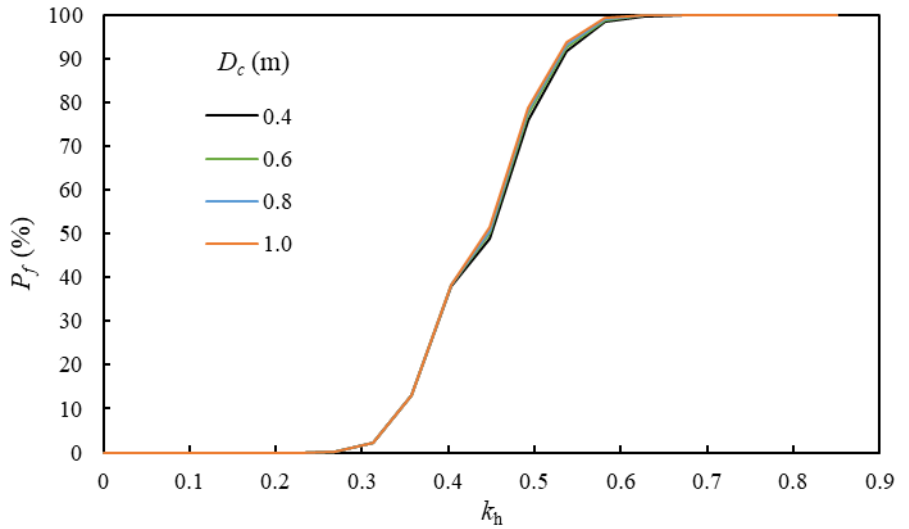


Fig. 9. Effect of D_c on failure probability.

4.3. Effect of T

Fig. 10 presents the effect of T on the P_f. The failure probability increased with increasing k_h and decreasing T. An increase in k_h directly leads to a significant rise in the tensile force demand that the geogrid must withstand. The tensile strength T determine the maximum confining stress it can provide. A decrease in T typically results in a reduced maximum allowable tensile force, increasing the failure probability.

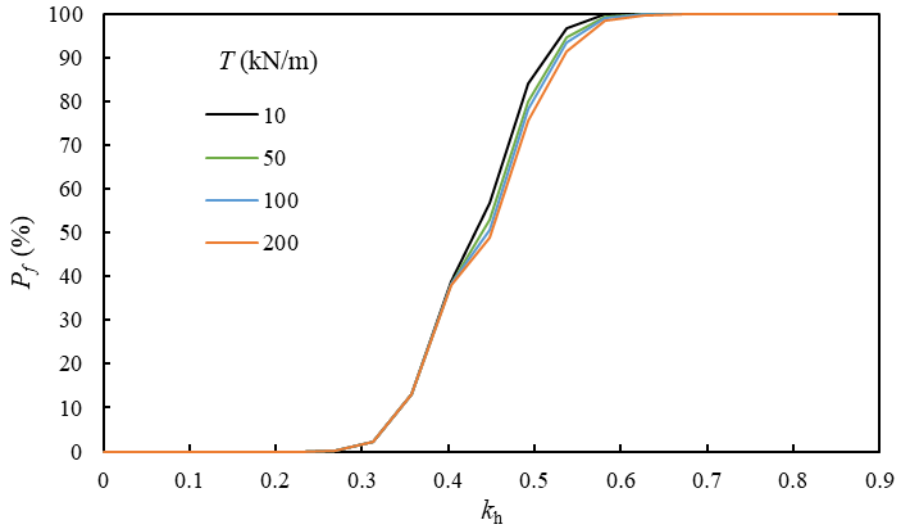


Fig. 10. Effect of T on failure probability.

4.4. Effect of m

Fig. 11 presents the effect of m on the P_f. The failure probability increased with decreasing m. A decrease in the m-value indicates that the total cross-sectional area of the column accounts for a smaller proportion within the treatment area. The vertical and horizontal loads will be primarily shared by the relatively weaker soil surrounding the columns. A low m-value indicates a sparse skeleton throughout the entire reinforced zone, resulting in diminished overall deformation and shear resistance. A low m-value delays the dissipation of pore water pressure during earthquakes, increasing the risk of soil liquefaction or softening. This coupled risk caused by the decrease in m increases the failure probability.

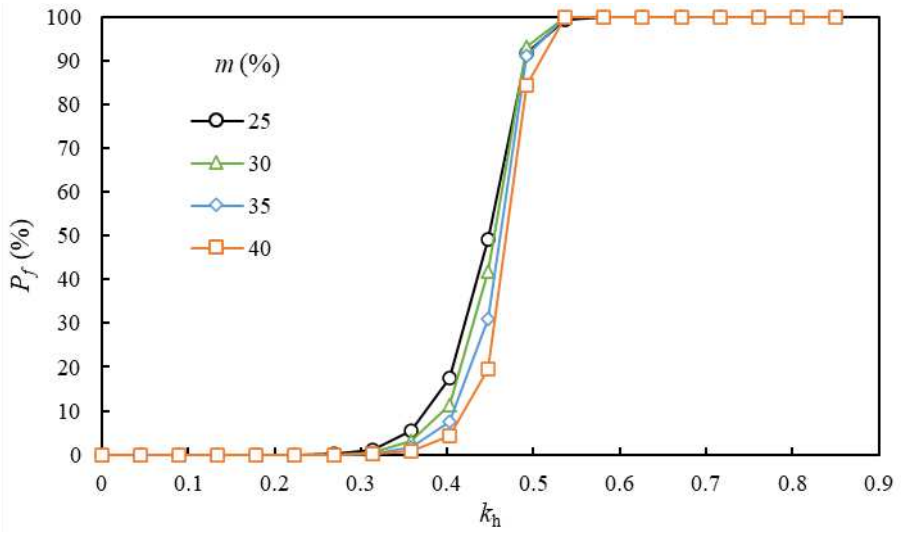


Fig. 11. Effect of m on failure probability.

4.5. Effect of Shear Strength

Fig. 12 (a), (b), (c), and (d) present the effect of φ_c, c_c, φ_s, and c_s on the P_f, respectively. The failure probability increased with decreasing φ_c, c_c, φ_s, or c_s. The P_f is more sensitive to internal friction angle than cohesion. The friction strength component of soil increases linearly with the increase in the confining pressure acting on the soil. In foundations, particularly under dynamic loads such as earthquakes, the confining pressure experienced by soil elements varies significantly. Therefore, even minor changes in the φ value are amplified by the confining pressure, exerting a substantial influence on the overall shear strength. However, the cohesion is considered an inherent strength independent of confining pressure. The failure typically manifests as deep shear failure, with the soil or column in this region subjected to elevated confining pressure. Consequently, variations in the internal friction angle directly and significantly alter the ultimate bearing capacity, thereby decisively influencing failure probability. The effect of shear strength (φ_s and c_s) of surrounding soil is more prominent than that of column material (φ_c and c_c). Even with GESC reinforcement, the majority of loads (particularly horizontal seismic loads) still need to be transmitted and dispersed through the surrounding soil. The overall instability of composite foundations typically originates from shear failure or excessive deformation of the surrounding soil. If the surrounding soil is inherently too weak (low φ_s and c_s), it will fail before effectively transmitting the load to the column. Consequently, the strength parameters of the surrounding soil directly determine the performance of the entire system.

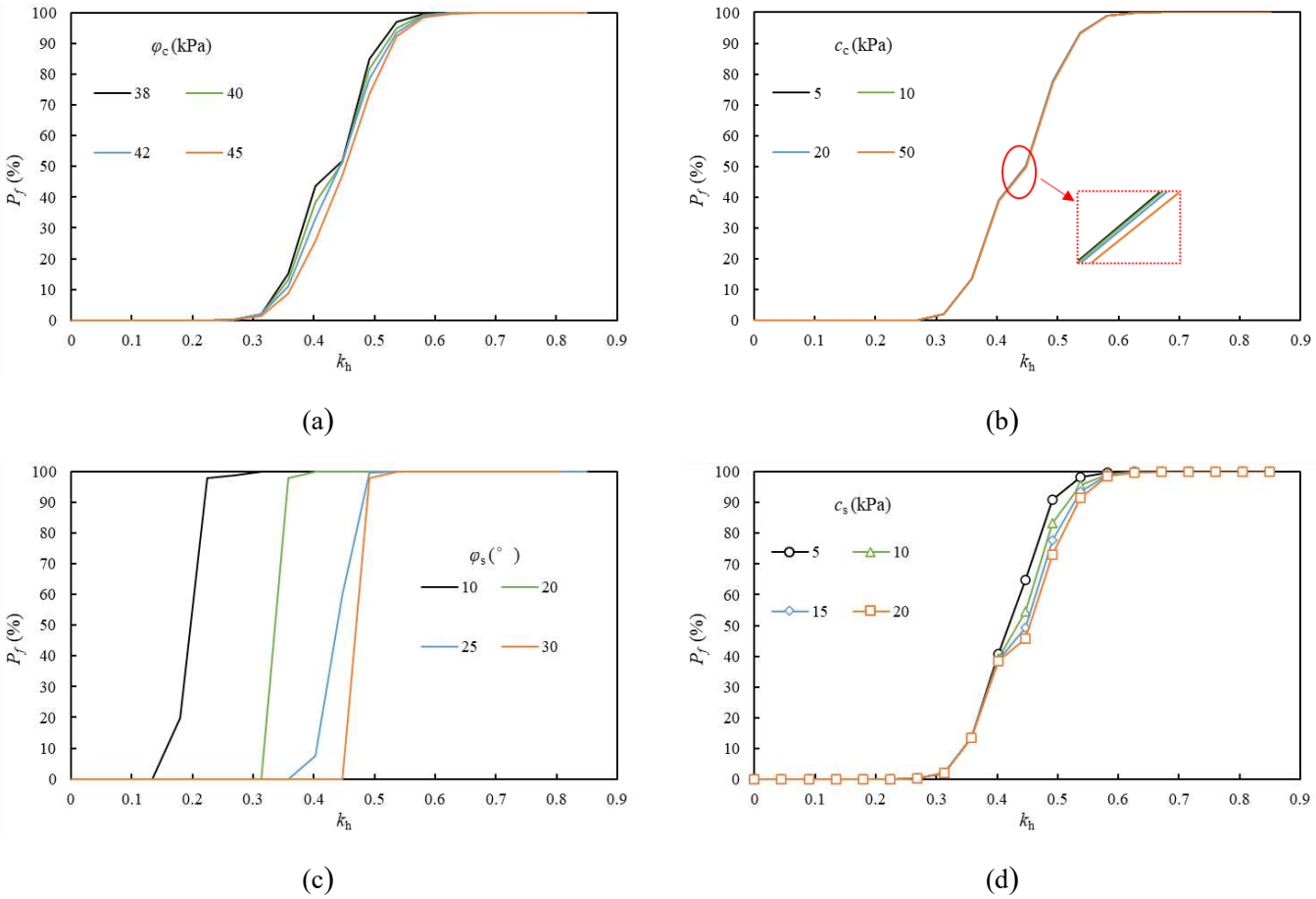


Fig. 12. Effect of shear strength on failure probability: (a) φ_c, (b) c_c, (c) φ_s, and (d) c_s.

4.6. Effect of P_v

Fig. 13 presents the effect of P_v on the P_f. The failure probability increased with increasing P_v. The vertical load demand represents the most direct demand acting on the foundation system. An increase in P_v elevates the internal stress levels in the foundation through multiple pathways, bringing them closer to the ultimate bearing state and thereby reducing the safety margin.

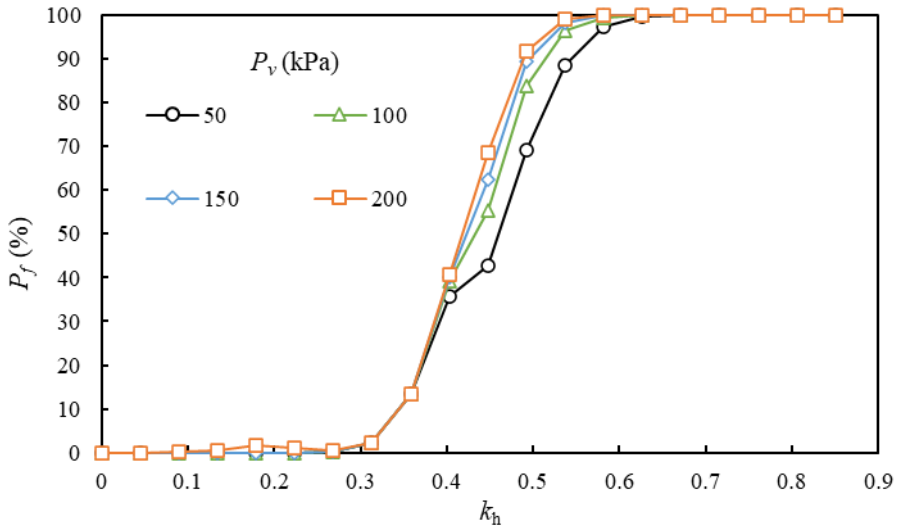


Fig. 13. Effect of P_v on failure probability.

4.7. Effect of B

Fig. 14 presents the effect of B on the P_f. A decrease in the B value significantly reduces anti-overturning and anti-slip capacity. The narrower the foundation width, the more concentrated the upper loads (including vertical and horizontal loads) become, resulting in excessive local stresses. Therefore, the failure probability increased with decreasing B.

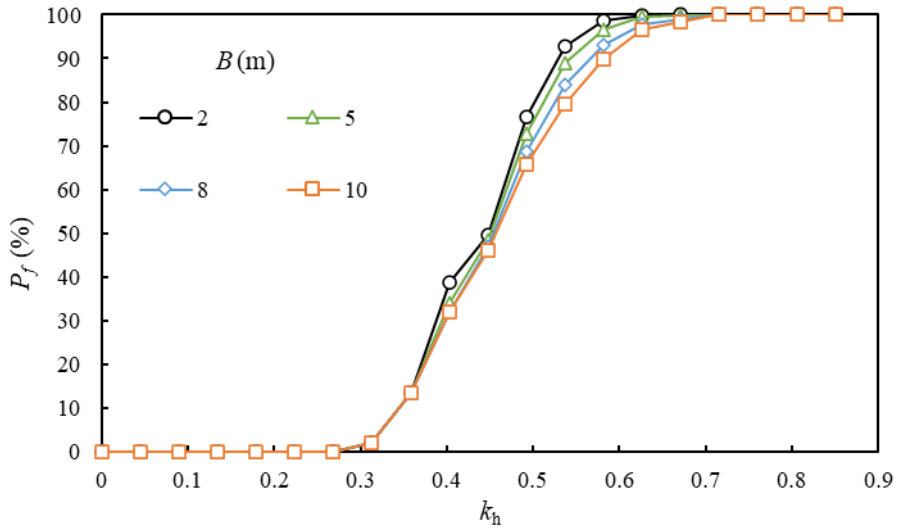


Fig. 14. Effect of B on failure probability.

4.8. Effect of q_1

Fig. 15 presents the effect of q_1 on the P_f. q_1 represents the self-weight pressure of the soil within the base embedded depth range (i.e., the overlying soil weight), enhancing the frictional anti-slip force between the foundation surface and the soil. A larger q_1 value increases the passive soil pressure, enabling more effective reduce of the foundation's horizontal displacement. Therefore, the failure probability decreased with increasing q_1.

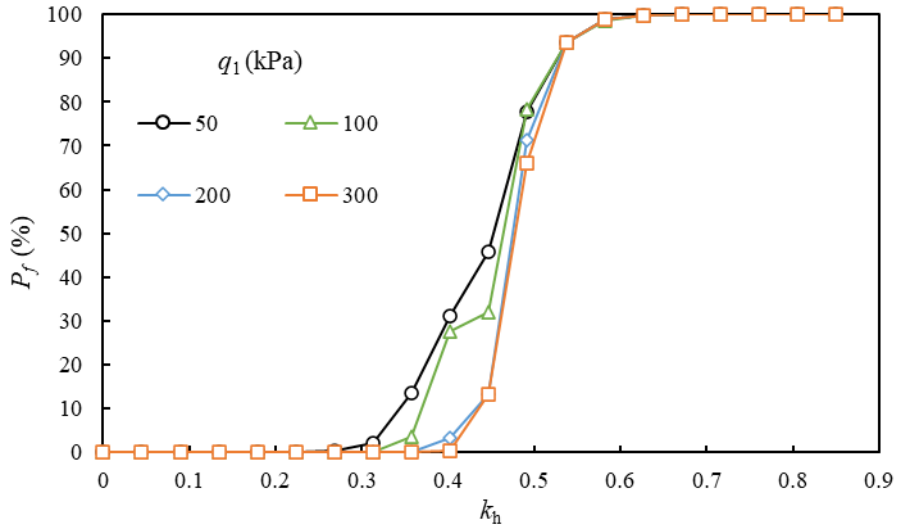


Fig. 15. Effect of q_1 on failure probability.

4.9. Effect of n

Fig. 16 presents the effect of n on the P_f. An increase in the shear strength utilization factor indicates that the shear strength of the composite zone is more fully mobilized and utilized under actual loading conditions, thereby directly enhancing the foundation's resistance to shear failure and improving its safety margin. Therefore, the failure probability decreased with increasing n.

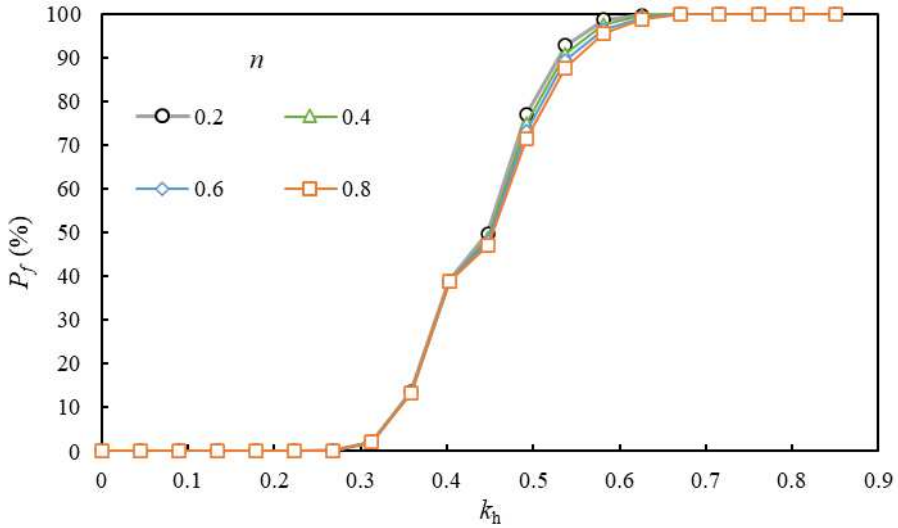


Fig. 16. Effect of n on failure probability.

5. Conclusions

A theoretical and probabilistic framework is developed for evaluating the ultimate seismic bearing capacity (q_u) and failure probability (P_f) of geogrid-encased stone column (GESC) composite foundations. The main conclusions are summarized as follows:

(1) The q_u and corresponding factors (N_{cE}, N_{qE}, and $N_{\gamma E}$) of GESC composite foundations are derived based on the equivalent area method and limit equilibrium theory. Three seismic bearing capacity factors are verified against several existing calculation methods. The calculated ultimate bearing capacity is further compared with experimental data from both shaking table and field tests.

(2) A machine learning-based probabilistic analysis model is established to quantify the seismic fragility of GESC composite foundations and provide a probabilistic basis for assessing the seismic performance of these foundations. The model is validated through comprehensive comparisons, including loss curves, accuracy curves, P_f curves, and ROC curves.

(3) Sensitivity analysis is conducted to investigate the effect of twelve parameters on the P_f. The P_f is positively correlated with parameters T, m, φ_c, c_c, φ_s, c_s, B, and q_1, but negatively correlated with k_v/k_h, D_c, and P_v. In contrast to the negligible influence of D_c and c_c, the parameters φ_s and k_v/k_h significantly govern the P_f.

(4) Compared to the improvement of column property and encasement strength, P_f of such foundations is more sensitive to the inherent properties of natural soil. The design shall prioritize the use of high-strength geogrids, ensure adequate foundation width, and maintain a high replacement rate—particularly by employing small-diameter columns in a dense arrangement—to comprehensively enhance seismic reliability.

Declaration of Competing Interest

The authors declare that they have no known competing financial interests or personal relationships that could have appeared to influence the work reported in this paper.

Data availability

Data will be made available on request.

References

Abid, M.S., Rathod, D., Vanapalli, S.K., (2023). "Bearing Capacity of Annulus Stone Column Double-Encapsulated with Geotextiles", *Int. J. Geomech.*, 23(2): 04022281. https://doi.org/10.1061/IJGNAI.GMENG-7817.

Alonso, J.A., Jimenez, R., (2011). Reliability Analysis of Stone Columns for Ground Improvement, GeoRisk 2011: risk assessment and Management. Reston, VA,

USA: Geotechnical Specia Publication 224, pp. 493-500.

Bahi, S., Houhou, M.N., (2024). “Optimizing ground improvement with encased stone columns: a 3D numerical analysis in very soft clay”, *World J. Eng.*, ahead-of-print(ahead-of-print). https://doi.org/10.1108/WJE-12-2023-0516.

Bahrami, M., Marandi, S.M., (2021). “Large-Scale Experimental Study on Collapsible Soil Improvement Using Encased Stone Columns”, *Int. J. Eng.*, 34(5): 1145-1155. https://doi.org/10.5829/ije.2021.34.05b.08.

Bazzazian Bonab, S., Lajevardi, S.H., Saba, H.R., Ghalandarzadeh, A., Mirhosseini, S.M., (2020). “Experimental studies on single reinforced stone columns with various positions of geotextile”, *Innovative Infrastruct. Solutions*, 5(3): 98. https://doi.org/10.1007/s41062-020-00349-0.

Bhandari, A., Han, J., (2010). “Investigation of geotextile–soil interaction under a cyclic vertical load using the discrete element method”, *Geotext. Geomembr.*, 28(1): 33-43. https://doi.org/10.1016/j.geotexmem.2009.09.005.

Budhu, M., Al-Karni, A., (1993). “Seismic bearing capacity of soils”, *Géotechnique*, 43(1): 181-187. https://doi.org/10.1680/geot.1993.43.1.181.

Cai, X., Zhang, L., Yang, Z., Mao, B., (2025). “Dynamic Behavior of GESC Groups in Sand Under Sinusoidal Loading: A Continuum-Discrete Coupled Analysis”, *Int. J. Numer. Anal. Methods Geomech.*, 49(11): 2655-2669. https://doi.org/10.1002/nag.4000.

Cai, X., Zhang, L., Yang, Z., Tan, J., Yue, S., (2026). “Seismic bearing capacity and fragility analysis of geogrid-encased stone column composite foundations”, *Geotext. Geomembr.*, 54(1): 99-114. https://doi.org/10.1016/j.geotexmem.2025.09.003.

Castro Gonzalez, J., Miranda Manzanares, M., Justo Urrutia, J., (2024). “An analytical solution for the settlement of encased stone columns beneath rigid footings”, *Geotext. Geomembr.*, 52(4): 451-464. https://doi.org/10.1016/j.geotexmem.2024.01.001.

Cengiz, C., Guler, E., (2018a). “Seismic behavior of geosynthetic encased columns and ordinary stone columns”, *Geotext. Geomembr.*, 46(1): 40-51. https://doi.org/10.1016/j.geotexmem.2017.10.001.

Cengiz, C., Guler, E., (2018b). “Shaking table tests on geosynthetic encased columns in soft clay”, *Geotext.*

Geomembr., 46(6): 748-758. https://doi.org/10.1016/j.geotexmem.2018.07.009.

Cengiz, C., Guler, E., (2020). "Load bearing and settlement characteristics of Geosynthetic Encased Columns under seismic loads", *Soil Dyn. Earthquake Eng.*, 136: 106244. https://doi.org/10.1016/j.soildyn.2020.106244.

Chen, J.-F., Zhang, X., Yoo, C., Gu, Z.-A., (2022). "Effect of basal reinforcement on performance of floating geosynthetic encased stone column-supported embankment", *Geotext. Geomembr.*, 50(4): 566-580. https://doi.org/10.1016/j.geotexmem.2022.01.006.

Dinesh, N., Banerjee, S., Rajagopal, K., (2024). "3D numerical analysis of liquefaction mitigation using ordinary and encased granular columns", *Soil Dyn. Earthquake Eng.*, 181: 108680. https://doi.org/10.1016/j.soildyn.2024.108680.

Elwakeel, A.O., Elsherbini, R.M., (2024). "Effect of Column Material Internal Angle of Friction and the Geotextile Stiffness on the Behavior of Group of Geosynthetic-Encased Stone Column", *Indian Geotech. J.* https://doi.org/10.1007/s40098-024-01005-5.

Farah, R.E., Nalbantoglu, Z., (2020). "Behavior of geotextile-encased single stone column in soft soils", *Arabian J. Sci. Eng.*, 45(5): 3877-3890. https://doi.org/10.1007/s13369-019-04299-3.

Geng, L., Tang, L., Cong, S.Y., Ling, X.Z., Lu, J., (2017). "Three-dimensional analysis of geosynthetic-encased granular columns for liquefaction mitigation", *Geosynth. Int.*, 24(1): 45-59. https://doi.org/10.1680/jgein.16.00014.

Gu, M., Cai, X., Lu, Y., Han, D., (2025). "Numerical investigation of cyclic load effects on geogrid-encased stone columns using a 3D coupled method", *Soil Dyn. Earthquake Eng.*, 193: 109332. https://doi.org/10.1016/j.soildyn.2025.109332.

Gu, M., Cui, J., Yuan, J., Wu, Y., Li, Y., Mo, H., (2022a). "The stress and deformation of stone column-improved soft clay by discrete element modelling", *Eur. J. Environ. Civ. Eng.*, 26(4): 1544-1560. https://doi.org/10.1080/19648189.2020.1715851.

Gu, M., Han, J., Zhao, M., (2020). "Three-Dimensional DEM Analysis of Axially Loaded Geogrid-Encased Stone Column in Clay Bed", *Int. J. Geomech.*, 20(3): 1-11. https://doi.org/10.1061/(asce)gm.1943-5622.0001595.

Gu, M., Mo, H., Qiu, J., Yuan, J., Xia, Q., (2022b). "Behavior of floating stone columns reinforced with geogrid encasement in model tests", *Front. Mater.*, 9: 1-10. https://doi.org/10.3389/fmats.2022.980851.

Gu, M., Zhao, M., Zhang, L., Han, J., (2016). "Effects of geogrid encasement on lateral and vertical deformations of stone columns in model tests", *Geosynth. Int.*, 23(2): 100-112. https://doi.org/10.1680/jgein.15.00035.

Hassen, G., Gueguin, M., de Buhan, P., (2013). "A homogenization approach for assessing the yield strength properties of stone column reinforced soils", *Eur. J. Mech. A. Solids*, 37: 266-280. https://doi.org/10.1016/j.euromechsol.2012.07.003.

Hosseinpour, I., (2024). "Three-Dimensional Numerical Analysis of Embankment Overlying Geotextile-Encased Columns with Granular Platform", *Iranian Journal of Science and Technology, Transactions of Civil Engineering*, 48(3): 1641-1653. https://doi.org/10.1007/s40996-024-01390-0.

Ji, M., Li, F., Zheng, Y., (2025). "Influence of Geosynthetic Encasement Stiffness on the Deformation Behavior of Geosynthetic Encased Stone Columns Composite Foundation Under Dynamic Loading", *Proceedings of the 5th International Conference on Transportation Geotechnics (ICTG) 2024, Volume 8*, Singapore.

Ji, M., Wang, J., Zhao, Y., Deng, J., Zheng, Y., (2024). "Numerical Simulation of the Load Transfer Mechanism of a Geosynthetic Encased Stone Column Unit Cell under Embankment Loading", *Int. J. Geomech.*, 24(8): 04024162. https://doi.org/10.1061/IJGNAI.GMENG-9393.

Kang, B.-w., Wang, J.-q., Zhou, Y.-w., Lin, Z.-n., (2024). "Experimental analysis of compression bearing characteristics of multi-layer geogrid-encased aggregate column based on digital image measurement technology", *Constr. Build. Mater.*, 417: 135292. https://doi.org/10.1016/j.conbuildmat.2024.135292.

Kong, G., Zhou, Y., Liu, H., (2018). "Nonlinear Model Analysis of Radial Bulging Deformation of Geosynthetic-Encased Stone Columns", *Int. J. Geomech.*, 18(10): 06018022. https://doi.org/10.1061/(ASCE)GM.1943-5622.0001195.

Lakkimsetti, B., Latha, G.M., (2024). "Physico-mechanical aspects of liquefaction risk reduction in sand using geotextile-encased granular columns", *Acta Geotech.*, 19(10): 6843-6864. https://doi.org/10.1007/s11440-024-02402-z.

Liu, F., Guo, P., Hu, X., Li, B., Hu, H., Gong, X., (2023). "A DEM Study on Bearing Behavior of Floating Geosynthetic-Encased Stone Column in Deep Soft Clays", *Applied Sciences*, 13(11): 6838. https://doi.org/10.3390/app13116838.

Mahawish, A., Bouazza, A., Gates, W.P., (2021). "Model tests on biogrouted granular columns in soft soil", *Can. Geotech. J.*, 58(12): 1791-1800. https://doi.org/10.1139/cgj-2020-0361.

Menon, A.R., Bhasi, A., (2024). "Evaluation of Critical Length of Encasement for Stone Column-Supported Embankment with Basal Geocell", *Arabian J. Sci. Eng.*, 49: 13821–13843. https://doi.org/10.1007/s13369-024-08778-0.

Modalavalasa, U., Ramanathan, A., (2024). "Performance of Encased Stone Column Aggregates Using Large-Scale Triaxial Testing", *Geo-Congress 2024*,

Mohamed, M.K., Sakr, M.A., Azzam, W.R., (2023). "Geotechnical behavior of encased stone columns in soft clay soil", *Innovative Infrastruct. Solutions*, 8(2): 80. https://doi.org/10.1007/s41062-023-01044-6.

Nav, M.A., Rahnavard, R., Noorzad, A., Napolitano, R., (2020). "Numerical evaluation of the behavior of ordinary and reinforced stone columns", *Structures*, 25: 481-490. https://doi.org/10.1016/j.istruc.2020.03.021.

Nayak, S., Balaji, M., Preetham, H.K., (2020). "A Study on the Behaviour of Stone Columns in a Layered Soil System", *Transp. Infrastruct. Geotechnol.*, 7(1): 85-102. https://doi.org/10.1007/s40515-019-00090-x.

Nayak, S., Vibhoosha, M.P., Bhasi, A., (2019). "Effect of Column Configuration on the Performance of Encased Stone Columns with Basal Geogrid Installed in Lithomargic Clay", *Int. J. Geosynth. Ground Eng.*, 5(4): 29. https://doi.org/10.1007/s40891-019-0181-y.

Ou Yang, F., Fan, G., Wang, K., Yang, C., Lyu, W., Zhang, J., (2021). "A large-scale shaking table model test for acceleration and deformation response of geosynthetic encased stone column composite ground", *Geotext. Geomembr.*, 49(5): 1407-1418. https://doi.org/10.1016/j.geotexmem.2021.05.013.

Pandey Balbir, K., Rajesh, S., Chandra, S., (2024). "Electrokinetics in a Stone Column Encased by a Conductive Jute Geotextile: The Role of Anode Materials", *Int. J. Geomech.*, 24(6): 04024095. https://doi.org/10.1061/IJGNAI.GMENG-9545.

Pandey, B.K., Rajesh, S., Chandra, S., (2020). "Numerical Evaluation of Geogrid-Encased Stone Columns in

435 Soft Soil under Embankment Loading", *Geo-Congress*: 543-551.
436 https://ascelibrary.org/doi/10.1061/9780784482780.053.
437 Pandey, B.K., Rajesh, S., Chandra, S., (2022). "Time-Dependent Behavior of Embankment Resting on Soft
438 clay Reinforced with Encased Stone Columns", *Transp. Geotech.*, 36: 100809.
439 https://doi.org/10.1016/j.trgeo.2022.100809.
440 Pulko, B., Logar, J., (2017). "Fully coupled solution for the consolidation of poroelastic soil around
441 geosynthetic encased stone columns", *Geotext. Geomembr.*, 45(6): 616-626.
442 https://doi.org/10.1016/j.geotexmem.2017.08.003.
443 Qin, X.Z., Chen, J.F., He, P.C., (2024). "Numerical simulation of bending characteristics of geosynthetic
444 encased stone column", *IOP Conf. Ser.: Earth Environ. Sci*, 1335(1): 012018.
445 https://doi.org/10.1088/1755-1315/1335/1/012018.
446 Qiu, R., Gou, J., Liu, K., El Naggar, M.H., Xiao, K., Zheng, L., Wang, T., (2025). "Seismic fragility analysis
447 of geosynthetic-encased stone column composite foundation", *Soil Dyn. Earthquake Eng.*, 189: 109095.
448 https://doi.org/10.1016/j.soildyn.2024.109095.
449 Rathod, D., Abid, M.S., Vanapalli, S.K., (2021). "Performance of polypropylene textile encased stone
450 columns", *Geotext. Geomembr.*, 49(1): 222-242. https://doi.org/10.1016/j.geotexmem.2020.10.025.
451 Richards, R., Elms, D.G., Budhu, M., (1993). "Seismic Bearing Capacity and Settlements of Foundations",
452 *Journal of Geotechnical Engineering*, 119(4): 662-674. https://doi.org/10.1061/(ASCE)0733-
453 9410(1993)119:4(662).
454 Sadr, A., Hataf, N., (2021). "Experimental and analytical study on soilbag and encased sand columns in loose
455 sand", *Transp. Geotech.*, 29: 100553. https://doi.org/10.1016/j.trgeo.2021.100553.
456 Soubra, A.-H., (1997). "Seismic bearing capacity of shallow strip footings in seismic conditions",
457 *Geotechnical Engineering, Institution of Civil Engineers*, 125: 230-241.
458 https://doi.org/10.1680/igeng.1997.29659.
459 Tan, X., Hu, Z., Cao, M., Chen, C., (2020). "3D discrete element simulation of a geotextile-encased stone
460 column under uniaxial compression testing", *Comput. Geotech.*, 126: 103769.
461 https://doi.org/10.1016/j.compgeo.2020.103769.

462 Tang, L., Cong, S., Ling, X., Lu, J., Elgamal, A., (2015). "Numerical study on ground improvement for
463 liquefaction mitigation using stone columns encased with geosynthetics", *Geotext. Geomembr.*, 43(2):
464 190-195. https://doi.org/10.1016/j.geotexmem.2014.11.011.
465 Thakur, A., Rawat, S., Gupta, A.K., (2020a). "Experimental and numerical modelling of group of
466 geosynthetic-encased stone columns", *Innovative Infrastruct. Solutions*, 6(1): 12.
467 https://doi.org/10.1007/s41062-020-00379-8.
468 Thakur, A., Rawat, S., Gupta, A.K., (2020b). "Experimental study of ground improvement by using encased
469 stone columns", *Innovative Infrastruct. Solutions*, 6(1): 1. https://doi.org/10.1007/s41062-020-00383-y.
470 Yoo, C., Abbas, Q., (2019). "Performance of geosynthetic-encased stone column-improved soft clay under
471 vertical cyclic loading", *Soils Found.*, 59(6): 1875-1890. https://doi.org/10.1016/j.sandf.2019.08.006.
472 Yoo, C., Abbas, Q., (2020). "Laboratory investigation of the behavior of a geosynthetic encased stone column
473 in sand under cyclic loading", *Geotext. Geomembr.*, 48(4): 431-442.
474 https://doi.org/10.1016/j.geotexmem.2020.02.002.
475 Yoosefi, S., Meehan, C.L., Garakani, A.A., Mosalmanzadeh, A., (2024). "Bearing Capacity of a Stone Column
476 Constructed Using the Vibro-Replacement Method: Experimental and Numerical Investigations", *Geo-*
477 *Congress 2024*,
478 Yousuf, S., Samadhiya, N.K., (2024). "Numerical Evaluation of Pile Length, Lateral Bulging and Encasement
479 Length: A Comparative Study on Ordinary and Encased Granular Piles", *Int. J. Geosynth. Ground Eng.*,
480 10(3): 48. https://doi.org/10.1007/s40891-024-00556-0.
481 Zeini, H.A., Lwti, N.K., Imran, H., Henedy, S.N., Bernardo, L.F.A., Al-Khafaji, Z., (2023). "Prediction of the
482 bearing capacity of composite grounds made of geogrid-reinforced sand over encased stone columns
483 floating in soft soil using a White-box machine learning model", *Applied Sciences*, 13(8): 5131.
484 https://doi.org/10.3390/app13085131.
485 Zhang, L., Cai, X., Yang, Z., (2025). "Dynamic Response of GESCs-Supported Embankments in Sand Under
486 Sinusoidal Loading: A Fluid-Solid Coupling Method", *Int. J. Numer. Anal. Methods Geomech.*, 49(16):
487 4001-4019. https://doi.org/10.1002/nag.70055.
488 Zhang, L., Peng, B., Zhou, S., Cui, P., Liu, Y., (2024). "Numerical study on stability of geosynthetic-encased

stone column-supported embankments based on equivalent method", *Comput. Geotech.*, 169: 106179. https://doi.org/10.1016/j.compgeo.2024.106179.

Zhang, W., Luo, Q., Jiang, L., Li, A., Luo, F., (2017). "Variation characterization and type classification of soil strength parameters based on reliability index", *Yanshilixue Yu Gongcheng Xuebao/Chinese Journal of Rock Mechanics and Engineering*, 36: 4188-4204. https://doi.org/10.13722/j.cnki.jrme.2016.1623.

Zhang, Y., Chan, D., Wang, Y., (2012). "Consolidation of composite foundation improved by geosynthetic-encased stone columns", *Geotext. Geomembr.*, 32: 10-17. https://doi.org/10.1016/j.geotexmem.2011.10.006.

Zheng, G., Xia, B., Zhou, H., Zhao, J., Yu, X., Sun, X., Du, J., (2020). "Seismic Bearing Capacity of Strip Footings on Ground Reinforced by Stone Columns Using Upper-Bound Solutions", *Int. J. Geomech.*, 20(9): 06020024. https://doi.org/10.1061/(ASCE)GM.1943-5622.0001794.

Zhou, Y., Kong, G., Peng, H., Li, C., Qin, H., (2019). "Visualization of bulging development of geosynthetic-encased stone column", *Geomech. Eng.*, 18(3): 329-337.